AIMS Materials Science, 6(4): 484–497.
DOI: 10.3934/matersci.2019.4.484
Received: 05 April 2019
Accepted: 05 June 2019
Published: 14 June 2019

http://www.aimspress.com/journal/Materials

Research article

Evolution of activation energy during hot deformation of Al–15% B_4C composites containing Sc and Zr

Jian Qin[1,2], Zhan Zhang[1] and X.-Grant Chen[1,*]

[1] Department of Applied Science, University of Quebec at Chicoutimi, Saguenay (QC), Canada G7H 2B1
[2] High-performance metal structural materials research institute, Soochow University, Suzhou, 215021, China

*** Correspondence:** Email: xgrant_chen@uqac.ca; Tel: 14185455011 ext. 2603.

Abstract: During hot deformation, the activation energy, Q, is an essential parameter that indicates the difficulty level in the hot working processing. The evolution of the activation energies of three Al–15% B_4C composites (the base material, S40 with 0.4% Sc and SZ40 with 0.4% Sc and 0.2% Zr) was investigated using high-temperature flow stress data based on a revised Sellar's constitutive equation. The microstructure evolution during hot deformation was characterized using a transmission electron microscope. The calculated activation energy maps reveal that the activation energy during hot deformation was related to the microstructure change in addition to deformation conditions. For the base composite, the variation of the activation energy was small because the microstructure barely changed during deformation. For the Sc and Zr containing composites (S40 and SZ40), dynamic precipitation occurred at high deformation temperature and the activation energy map can be divided in two regions. The activation energy decreases with an increase of deformation temperature to the minimum level in the region I where the composites were in the solid solution condition. It follows by an increase with increasing temperature in the region II where dynamic precipitation occurred. Based on the combination of the activation energy map with the flow instability zone, the optimum hot workability of a composite in term of excellent processability was proposed at the domain where the less energy of hot deformation was required.

Keywords: Al–B_4C composites; activation energy map; high-temperature flow stress; Sc and Zr

addition; dynamic precipitation

1. Introduction

Al–B_4C metal matrix composites have been applied in the nuclear industry as neutron absorber materials for the storage of used nuclear fuels, due to their lightweight, good mechanical properties and excellent neutron absorption capability of incorporated boron carbides (B_4C) [1]. Scandium (Sc) and zirconium (Zr) are added in Al–B_4C composites to improve the thermal stability and increase mechanical properties at elevated temperature, as they can form fine and coarsening-resistant Al_3Sc and Al_3(Sc,Zr) coherent nanoscale precipitates [2,3]. Al-based metal matrix composites are often fabricated by thermomechanical processing in the form of rolling and extrusion. The hot deformation behavior of those composites is mostly influenced by the alloy chemistry and microstructure during thermomechanical processing. In our previous works [4–8], the mechanical properties, microstructure evolution and hot deformation behavior of Al–B_4C composites containing Sc and Zr were explored. To understand the hot deformation behavior of materials, Arrhenius-type constitutive equations are widely used to establish the relationship between the flow stress, deformation temperature and strain rate during hot deformation [9] and to calculate the activation energy [10]. The activation energy for hot deformation, *Q*, is an essential parameter that indicates the difficulty level in the hot working processing.

Most of previous studies treated *Q* as a constant under applied hot deformation conditions for a specific material [7,11,12]. However, *Q* mainly reflects the free energy barrier to dislocation slipping, which is affected by the deformation temperature and external stress [13,14]. In the previous work of our group [14], Shi et al. proposed a revised Sellars' constitutive equation to relate *Q* to the deformation temperature (T) and the strain rate ($\dot{\varepsilon}$). Using this novel concept, the activation energy maps of 7150 alloy were constructed [15]. In recent works [16,17], the activation energy map was associated with the processing map to optimize the hot work windows of 7050 alloy. Malas et al. [18] explored the concept of the superposition of the activation energy map with the stability map for identifying the safe hot work zones of 2024-20 vol% SiC composites. However, very few works focused on the application of the activation energy map to study the hot workability caused by the microstructure change during hot deformation.

Several previous works have reported that dynamic precipitation can occur during hot deformation in Al–Zn–Mg–Cu 7xxx alloys [11,15], Al–Mg–Si–Cu 6xxx alloys [19] and Al–Cu–Mg 2xxx alloys [20]. In addition, the activation energy of precipitation-strengthening aluminum alloys in a solution condition often shows a higher value than that in a precipitation condition. Zhang et al. [21] found that the activation energy of Al–Mg–Si–Cu alloys in pre-aged condition with precipitation ranged 150–205 kJ/mol, whereas the activation energy in solution condition was determined to be higher than 285 kJ/mol. The activation energy variation would be related to microstructure change, especially dynamic precipitation. Cerri et al. [22] also reported that the activation energy of solution-treated Al–Zn–Mg–Cu alloys was approximately 50% higher than that in the precipitated condition.

In the present work, the evolution of the activation energy of Al–15 vol% B_4C composites containing Sc and Zr under different temperatures and strain rates was derived by constitutive analyses. The dynamic precipitation of these composites during hot deformation was investigated under various deformation conditions using a transmission electron microscope (TEM). The relation between the activation energy, microstructure and processability was discussed.

2. Experimental procedure

Three Al–B_4C composites, namely the base composite (AA1100 aluminum alloy with 15 vol% B_4C), S40 composite (AA1100–15 vol% B_4C with 0.4 wt% Sc) as well as SZ40 composite (AA1100–15 vol% B_4C with 0.4 wt% Sc and 0.24 wt% Zr), were prepared by the liquid-mixing process in this study. Their nominal chemical compositions are listed in Table 1. In the batch process, commercial pure aluminum (99.7%) was first melted in an electric resistance furnace. The master alloys and the prefabricated AA1100–25 vol% B_4C with 2.0 wt% Ti cast ingot were subsequently added to the melt. Ti was deliberately added to limit the interface reaction between B_4C particles and liquid aluminum during Al–B_4C composite preparation [6], and Ti was mostly consumed by the formation of TiB_2 layer on B_4C particle surfaces. The average size of B_4C particles (F360) of the three composites was approximately 23 μm. The details for preparing the experimental composites can be found in [7].

Table 1. Chemical compositions of three composites.

Composite	Elements				
	B_4C	Ti	Sc	Zr	Al
Base	15 vol%	1.5 wt%	–	–	Bal.
S40	15 vol%	1.5 wt%	0.4 wt%	–	Bal.
SZ40	15 vol%	1.5 wt%	0.4 wt%	0.24 wt%	Bal.

The cast composites containing Sc and Zr (S40 and SZ40) were solution-treated at 640 ℃ for 24 and 96 hours, respectively, and then directly quenched in water. The base composite did not need the heat treatment, because AA1100 pure aluminum is non-heat-treatable. The details of the solution treatment for S40 and SZ40 composites were described in references [2–4,6–7]. The compression tests were performed in a Gleeble 3800 thermo-mechanical simulation unit at strain rates of 0.001–1 s^{-1} and deformation temperatures of 300–500 ℃, respectively. The cylindrical sample with a diameter of 10 mm and a length of 15 mm was used. During compression testing, all samples were heated to the desirable temperature at a constant rate of 10 ℃/s, and then held for 3 minutes to ensure a homogeneous temperature in the sample. The samples were compressed to a true strain of 0.8. In the compression test, a thermal couple was welded on the surface in the middle of the sample. Two graphic foils were placed on each side of the sample for lubrication.

For TEM specimen preparation, a plate with 500 μm thickness was first sliced from the sample, and then a few disks with 3 mm in diameter were punched form the plate. TEM specimens were

prepared by metallographic grinding, polishing and dimpling, followed by milling with a Gatan PIPS (Model 691).

The microstructure of deformed samples was studied using a transmission electron microscope (TEM, JEOL JEM-2100). For TEM observation, bright field images were taken on (111) plane and centered dark-field images of the precipitates were recorded using the {100} superlattice reflections near the <011> direction on two-beam diffraction conditions. The equivalent diameters of the precipitates were determined using image analysis on TEM images.

3. Results and discussion

3.1. High-temperature flow stress

The typical true stress–true strain plots obtained in the low and high temperature (300 and 450 ℃) under different strain rates for three composites are showed in Figure 1.

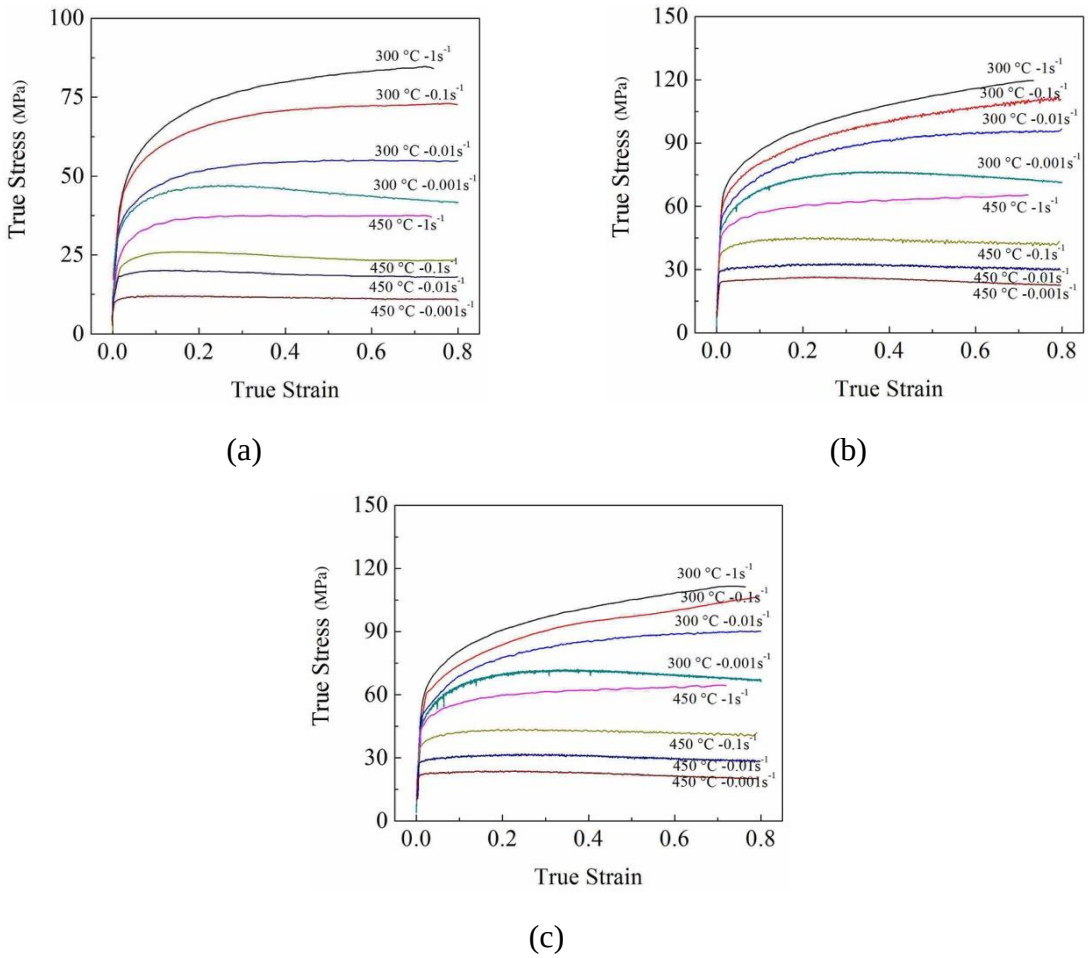

Figure 1. Typical true stress–true strain plots at two deformation temperatures and different strain rates: (a) the base composite, (b) S40 composite and (c) SZ40 composite.

In general, the flow stress increases rapidly at the beginning of the deformation, due to the work

hardening effect. After the rapid increase, the flow stress went more smoothly, in the most cases remained fairly constant because of the balance between dynamic softening and work hardening. The results indicate that the flow stresses of the base composite (Figure 1a) are obviously lower than that of the Sc and Zr containing composite (S40 in Figure 1b and SZ40 in Figure 1c) at all deformation conditions applied. The flow stresses of the composite containing Sc (S40) and the composite containing Sc and Zr (SZ40) are more and less close in most experimental conditions.

The peak flow stress evolutions of three composites as a function of the deformation temperature at various strain rates (0.001–1 s^{-1}) are illustrated in Figure 2.

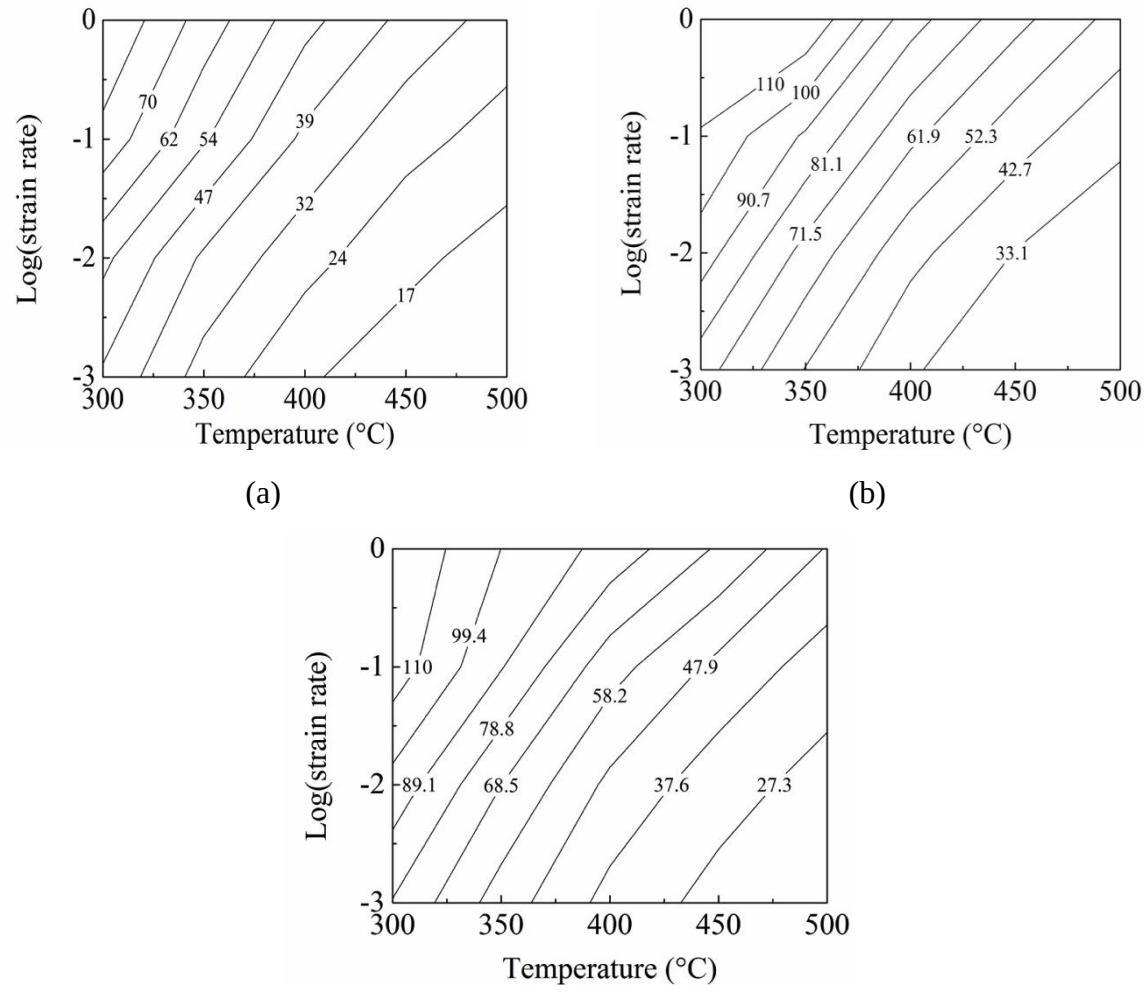

Figure 2. Evolution of peak flow stresses of Al–B_4C composites as a function of temperature and strain rate: (a) the base composite, (b) S40 composite and (c) SZ40 composite.

In the case that the flow stress curve remained fairly constant, the peak stress was taken as a constant value. In the other cases, the maximum stress value in the flow curve was taken as the peak stress. In the following section, the peak stresses are adopted in the calculation of constitutive equations of three composites. In general, the peak stress increases with an increase of the strain rate

and decreases with increasing deformation temperature. Under any given deformation condition, the peak stresses of S40 (Figure 2b) and SZ40 (Figure 2c) are obviously higher than that of the base composite (Figure 2a). It is evident that Sc and Zr in the composites considerably increase the resistance for the hot deformation.

3.2. Constitutive analysis

Various constitutive equations have been developed to analyze and predict the relationship between flow stress, strain rate and deformation temperature of engineering materials [9,23,24]. Among others, the hyperbolic-sine Arrhenius equation (the original Sellar's equation) is widely used, suitable in a wide range of stresses and strain rates [9]:

$$\dot{\varepsilon} = A\left[\sinh(\alpha\sigma)\right]^n \exp\left(-Q/RT\right) \tag{1}$$

where, $\dot{\varepsilon}$ is the strain rate (s^{-1}); σ is the flow stress (MPa); T is the deformation temperature (K); R is the universal gas constant (8.314 J mol^{-1} K^{-1}); Q is the activation energy for hot deformation (kJ mol^{-1}), and A, n and α are material constants.

From Eq 1, take nature logarithm and differentiating:

$$Q = R\left[\frac{\partial \ln \dot{\varepsilon}}{\partial \ln\left[\sinh(\alpha\sigma)\right]}\right]_T \left[\frac{\partial \ln\left[\sinh(\alpha\sigma)\right]}{\partial(1/T)}\right]_{\dot{\varepsilon}} = RnS \tag{2}$$

Inputting the experimental data of the high-temperature peak flow stresses of three composites, the material constants A, n, α and Q can be calculated [7] and the obtained values for the activation energy Q are presented in Table 2. As a traditional way, the Q is treated here as a constant. The Q of the base composite is 186.4 kJ/mol. The Q value of pure Al is in the range of 140–156 kJ/mol [25]. Compared to pure Al, Q of the base composite is approximately 35 kJ/mol higher, which is caused by a number of of B_4C particles in the aluminum matrix. With the addition of Sc and Zr, the Q value of S40 increases to 196.1 kJ/mol, and the value of SZ40 reaches 206.6 kJ/mol, confirming that Sc and Zr in Al–B_4C composites considerably increase the hot deformation resistance.

Table 2. Calculated activation energy for three composites.

Composites	Q (kJ mol^{-1})
Base	186.4
S40	196.1
SZ40	206.6

Recent research works [14–17] indicated that the activation energy for hot deformation of a material is not constant over a large range of temperature and strain rate. Shi et al. [14] proposed that the activation energy should be treated as a function of deformation temperature and strain rate using

a revised Sellar's constitutive equation:

$$\dot{\varepsilon} = A_{(T,\dot{\varepsilon})}\left[\sinh\left(\alpha\sigma\right)\right]^{n_{(T)}} \exp\left(-\frac{Q_{(T,\dot{\varepsilon})}}{RT}\right) \tag{3}$$

Similar as treated in Eq 2, Eq 3 can be rewritten as follows:

$$Q_{(T,\dot{\varepsilon})} = Rn_{(T)}S_{(\dot{\varepsilon})} \tag{4}$$

$n_{(T)}$ and $S_{\dot{\varepsilon}}$ are obtained from the slopes of the ln($\dot{\varepsilon}$)–ln[sinh(ασ$_p$)] plots at different deformation temperatures and the ln[sinh(ασ$_p$)]–1/T plots at various strain rates, respectively. From polynomial regression fitting, the relationships between n and temperature and between S and the strain rate are revealed in Figure 3. The values of n and S of the base composite are more and less stable. However, the trends of n and S changes in S40 and SZ40 composites are not monotonic.

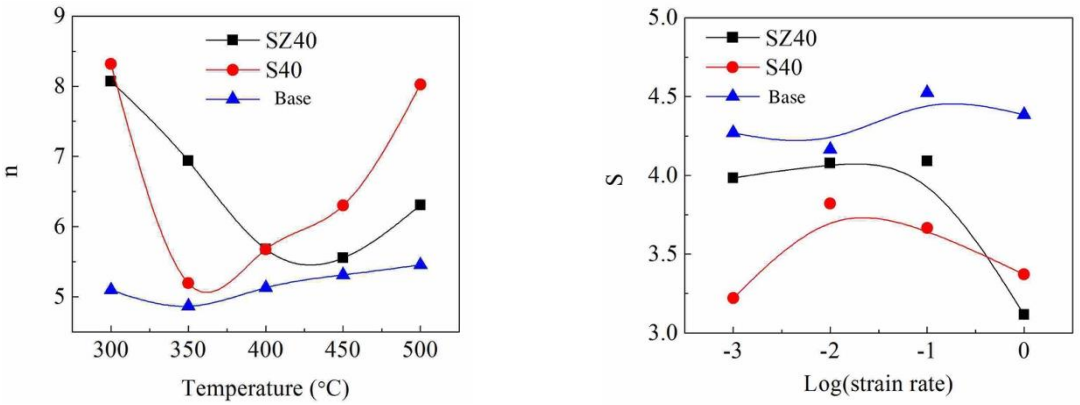

(a) (b)

Figure 3. Relationships between (a) *n* and *T* and (b) *S* and strain rate.

Then $Q_{(T,\dot{\varepsilon})}$ values can be calculated from the experimental data of $n_{(T)}$ and $S_{\dot{\varepsilon}}$ at each temperature and strain rate, and hence the corresponding *Q* maps for three composites can be established (Figure 4). It is evident that *Q* varies with deformation conditions (temperature and strain rate), but it behaves differently in three composites.

It can be seen that the *Q* values of the base composite only change from 170 to 200 kJ/mol. However, the *Q* values of S40 and SZ40 composites vary from 145 to 253 kJ/mol and 155 to 266 kJ/mol, respectively. It is apparent that the *Q* values of the base composite do not largely change and it may be treated as a constant, because the pure aluminum matrix and B_4C ceramic particles do not exhibit a significant microstructure change during hot deformation. However, there are large differences of *Q* values for S40 and SZ40 composites at various deformation conditions. The *Q* evolution for S40 and SZ40 composites can be divided into two regions. In the region I at the left side of Figure 4b (for S40) and 4c (for SZ40) where the temperature is below 365 and 425 ℃ respectively, *Q* of S40 and SZ40 decreases with increasing deformation temperature, until *Q*

approaches a valley where *Q* reaches the minimum value. In the region II at the right side of Figure 4b,c, *Q* of two composites recovers from the valley and increases with the increase of the deformation temperature. From our previous work [7], it is found that B_4C ceramic particles were very stable and barely changed during hot deformation of Al–B_4C composites. The large variation of *Q* in the composites containing Sc and Zr seems to be related to the microstructure change in the matrix at different deformation conditions.

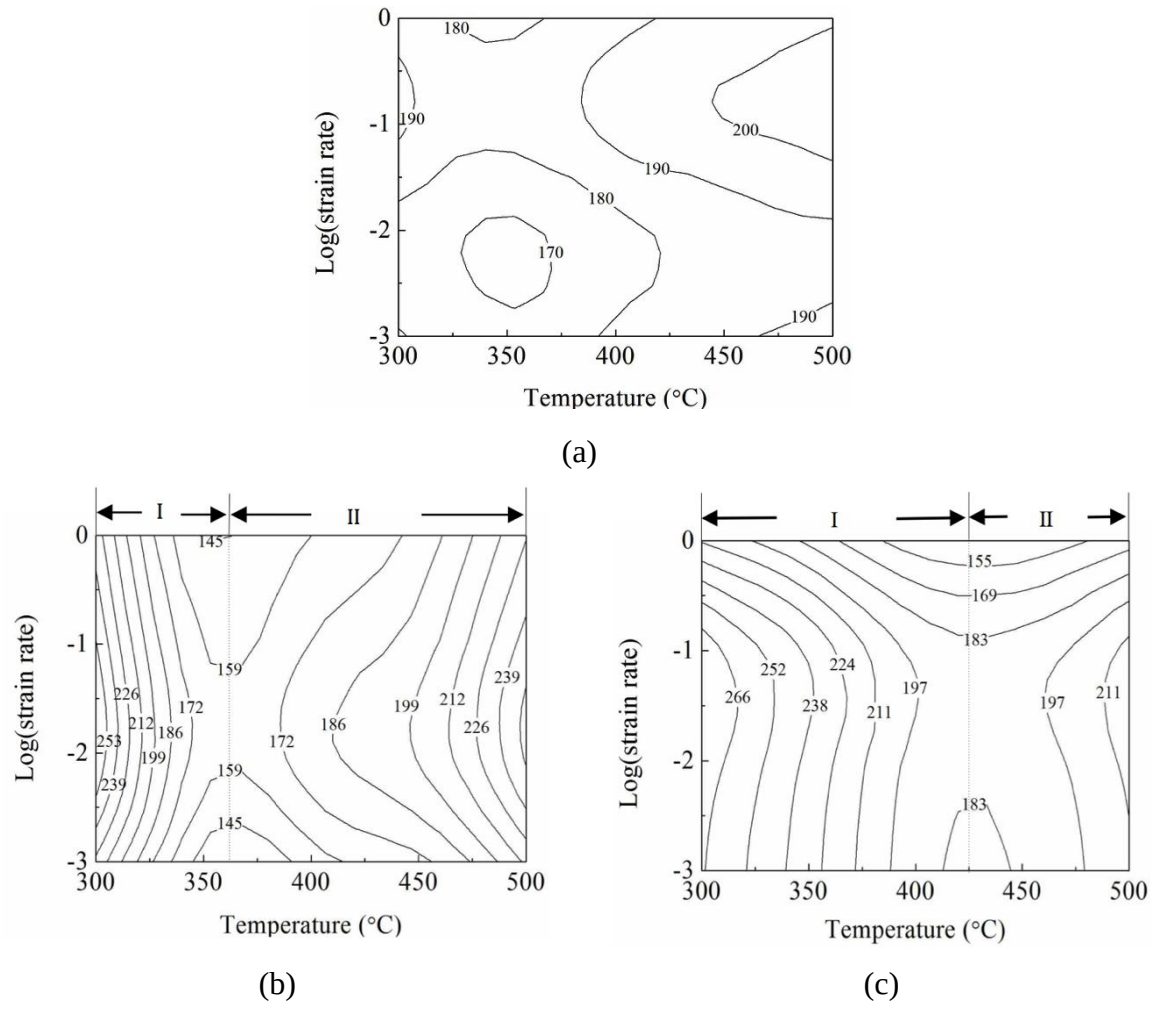

Figure 4. Activation energy maps for (a) the base, (b) S40 and (c) SZ40 composites.

3.3. Dynamic precipitation during hot deformation

After the solution treatment and before hot deformation, all Sc and Zr were dissolved in the aluminum matrix of S40 and SZ40 composites. Through a series of TEM examination at various deformation conditions, it was found that at high deformation temperatures (>375 ℃ in S40 and >425 ℃ in SZ40), a large number of Al_3Sc or $Al_3(Sc,Zr)$ nanoscale precipitates presented in the deformed microstructure of S40 and SZ40 composites, which indicates the dynamic precipitation during hot deformation. As an example, Figure 5a,b shows the TEM dark field images of S40 and SZ40 samples deformed at 500 ℃ with 1 s^{-1} strain rate, in which spherical precipitates are uniformly

distributed in the aluminum matrix. Al_3Sc in S40 and $Al_3(Sc,Zr)$ in SZ40 were identified by the selected area diffraction patterns and TEM-EDX analysis. The average precipitate radii of S40 and SZ40 composites are 9.8 and 5.4 nm, respectively. Figure 5c,d is TEM bright field images of S40 and SZ40 samples deformed at the same condition as Figure 5a,b, which reveal that the dislocations (white arrows) were pinned by precipitates (red arrows). With coarse precipitates in S40 (Figure 5c), dislocations tend to be tangled, while dislocations tend to be piled up with fine precipitates in SZ40 (Figure 5d).

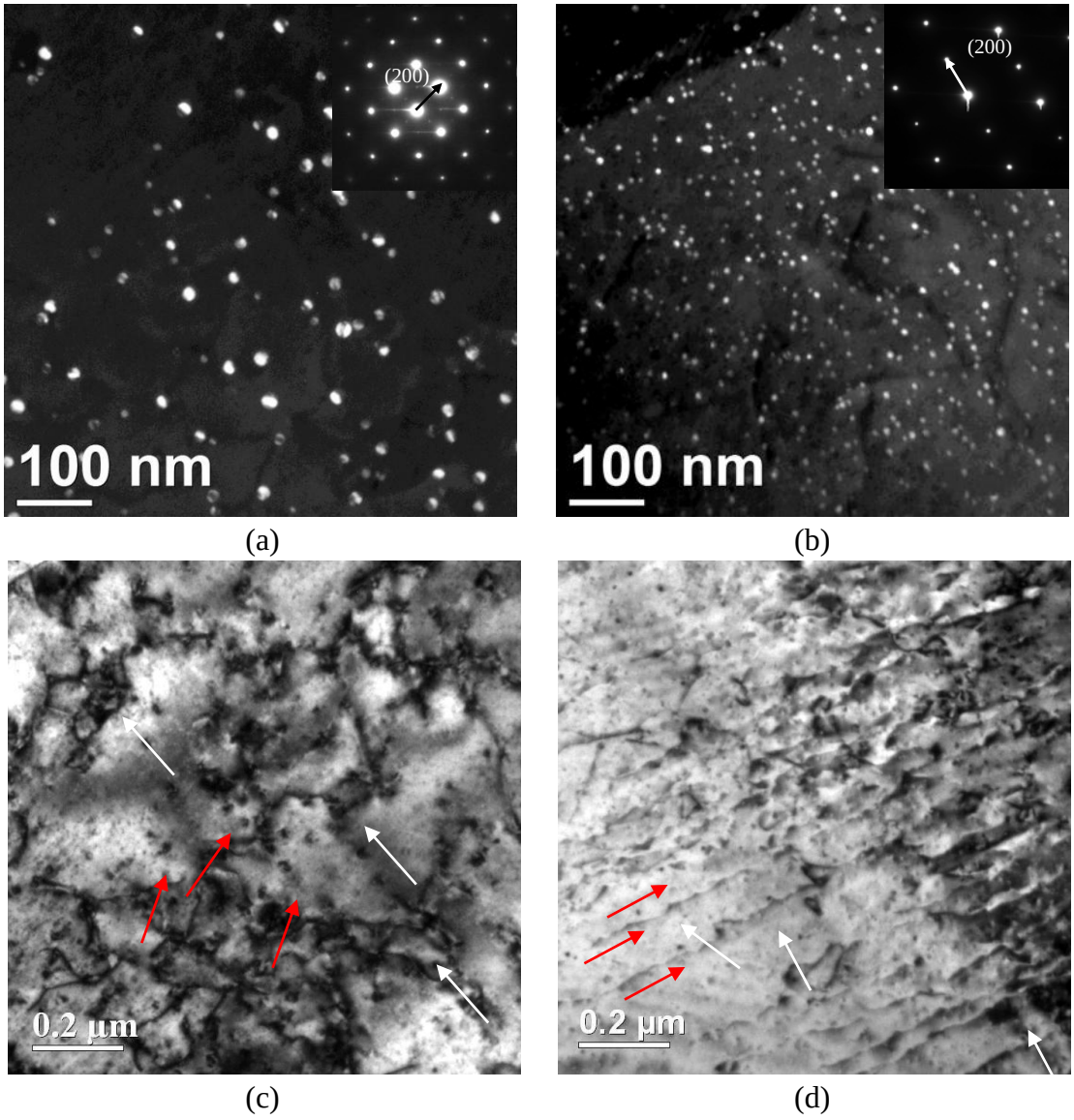

Figure 5. TEM images showing the precipitates and their interaction with dislocations, deformed at 500 ℃ with strain rate 1 s^{-1}: (a) Al_3Sc in S40, (b) $Al_3(Sc,Zr)$ in SZ40, and restricting the dislocation movement by precipitates in S40 (c) and SZ40 (d). The insets in (a) and (b) are the corresponding selected area electron diffraction patterns.

Figure 6 illustrates the evolution of precipitate size (radius) of Al_3Sc and $Al_3(Sc,Zr)$ for S40 and SZ40 composites at different hot deformation conditions. At low deformation temperature (the left

side of Figure 6), no precipitate has been observed in the deformed S40 and SZ40 composites. It indicates that all Sc and Zr are still in the supersaturated solid solution. On the right side of Figure 6 where the deformation temperature is high, dynamic precipitation occurs and the precipitate size increases with increasing deformation temperature. Due to lower diffusivity of Zr in aluminum than that of Sc, the coarsening of $Al_3(Sc,Zr)$ precipitates with the increase of temperature in SZ40 is slower than Al_3Sc precipitates in S40. Compared Figure 4 to Figure 6, it can be found that the trends of *Q* change in S40 and SZ40 are associated with the microstructure change, namely either Sc and Zr in solid solution or dynamic precipitation of Al_3Sc and $Al_3(Sc,Zr)$ during hot deformation.

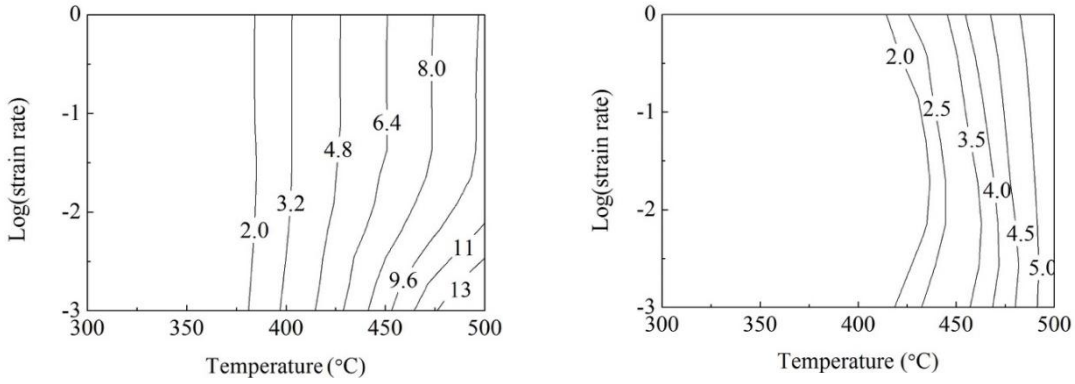

Figure 6. Evolution of precipitate size (radius) of Al_3Sc and $Al_3(Sc,Zr)$ at different hot deformation conditions: (a) S40 composite and (b) SZ40 composite.

In the region I of Figure 4b,c, both Sc and Zr solute atoms can act as the obstacles of dislocation movement. It is known that Sc and Zr solutes can diffuse to dislocations for an effective pinning. A moving dislocation can be dragged by the solute atoms during its slipping. In addition, solute atoms can bond with vacancies, reduces vacancy concentration and also brings in misfit strain field. For both conditions, it requires an extra energy for the dislocation movement under external load. Therefore, the *Q* values of S40 and SZ40 are much higher than that of the base composite. Compared to S40 composite, SZ40 composite contained more solute atoms, resulting in a higher *Q* than S40 at the same deformation condition. With the increase of deformation temperature, the dislocation movement becomes easier. Less energy is required to overcome the repulsion stress caused by solute atoms. Therefore, the *Q* continues to decrease with increasing deformation temperature to the minimum value where the valley between the region I and II lies. In SZ40 composite, due to a lower diffusivity of Zr in aluminum than Sc, the minimum value of *Q* moves to the high temperature side, and hence the region I of SZ40 (Figure 4c) is larger than that of S40 (Figure 4b).

In the region II of Figure 4b,c, the *Q* increases from its minimum value with the increase of deformation temperature as dynamic precipitation occurs. In this region, Al_3Sc and $Al_3(Sc,Zr)$ nanoscale precipitates act as obstacles to dislocation movement and subgrain boundary migration as Sc and Zr solute atoms were consumed by dynamic precipitation. In our recent work [6], it is proved the dislocation climbing mechanism is operative at elevated temperature (>250 ℃). In the climb model, dislocations need extra energy to form jogs in order to climb over the obstacles such as

precipitates. The larger those precipitates, more energy is required to form longer jogs. In addition, for the migration of subgrain boundaries, large precipitates require more energy to form new interfaces than small ones. Therefore, as the precipitates become coarser and fully come out with increasing temperature (Figure 6a,b), the *Q* increases correspondingly. In SZ40, because $Al_3(Sc,Zr)$ is more thermally stable than Al_3Sc, the precipitate size of $Al_3(Sc,Zr)$ only slightly increases with temperature, and hence the *Q* increases moderately with increasing temperature (Figure 4c) compared to that in S40 (Figure 4b).

It is interesting to note that the *Q* values in the region I (supersaturated solid solution condition) are generally higher than that in the region II (dynamic precipitation condition), indicating the composite in the solid solution condition is more difficult to deform than that in the precipitation condition. Similar phenomenon has also been found in AA2024 [26], AA7012 and AA7075 [22] and Al–Mg–Si–Cu alloys [21], in which the activation energies of those alloys in the solid solution condition exhibit higher values than that in the precipitation condition.

If *Q* is treated as a constant (Table 2), one can only obtain a general information that the hot workability of the composites containing Sc and Zr (S40 and SZ40) is somewhat worsen than that of the base composite. With the activation energy map (Figure 4), it can be seen that the *Q* values of S40 and SZ40 at the ends of both low and high temperature ranges (e.g., *Q* of S40 at 300–325 ℃ and 450–500 ℃ and *Q* of SZ40 at 300–375 ℃ and 475–500 ℃ respectively) are remarkably higher than that of the base composite. In other words, the hot deformation of S40 and SZ40 in such conditions is much more difficult compared to the other deformation conditions and to the base composite at the same deformation conditions. In the other hand, the *Q* values of S40 and SZ40 in the valley between the region I and II are in the minimum level and they are even lower than that of the base composite at the same deformation conditions, suggesting an ease deformation zone near the valley.

The processing map based on the dynamic material model (DMM) has been widely employed to study hot workability for aluminum alloys and Al-base metal matrix composites [27,28]. It can describe a flow instability zone and give optimum hot working windows based on the high efficiency of power dissipation. On the other hand, as *Q* represents the difficulty level of hot deformation, the *Q* map can indicate where (at which deformation conditions) the less energy is required and where is easy to deform. To better understand the hot workability in different aspects, the flow instability zone in the processing map for the same composites [7] is superposed on the *Q* maps, as shown in Figure 7. It can be seen that the flow instability zone (shaded domain) lies on the low temperature side of the region I where the *Q* values are higher than most of other regions, conforming the deformation is more difficult in the solid solution condition, particularly in the low temperature range. In addition, Al-based metal matrix composites are generally more difficult to deform compared to monolithic aluminum alloys. It is often desirable that the hot deformation, for instance of extrusion, can be taken place where the less energy is required due to the load capacity limit of the extrusion machine. Based on the minimum *Q* value and considering the industrial extrusion at relatively high strain rate, a domain (A) for easy deformation can be attractive for industrial applications (Figure 7). The domain A of S40 is situated at approximately *T* of 350–385 ℃ with $\dot{\varepsilon}$ of 0.1–1 s^{-1} (Figure 7a), while for SZ40 the domain A is located at *T* of 400–470 ℃ with $\dot{\varepsilon}$ of 0.3–1 s^{-1} (Figure 7b). The *Q* values in the domains A are even lower than the minimum *Q* value (170 kJ/mol) of the base composite (Figure 4a). It is reasonable to believe that the domains A in S40 and SZ40 in the valley zone are more

suitable to process. It is expected that the combination of the *Q* map with the flow instability zone can give a better guide to optimize the hot workability of a material in term of excellent processability.

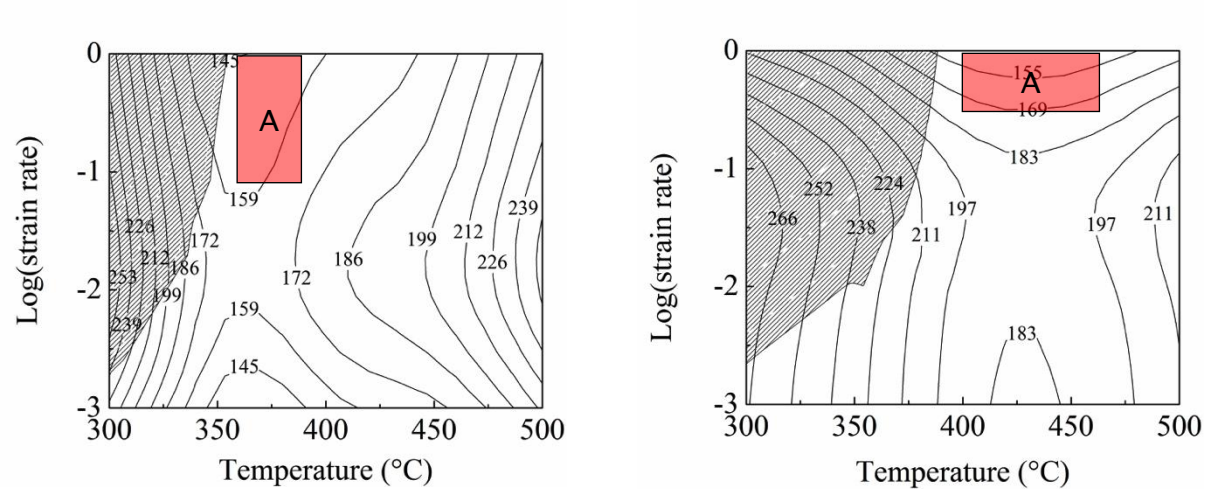

(a) (b)

Figure 7. Flow instability zone superposed on the *Q* maps: (a) S40 composite and (b) SZ40 composite.

4. Conclusions

(1) Using a revised Sellar's constitutive equation, the activation energy maps of three Al–15% B_4C composites were constructed. The activation energy was related to the microstructure change in the composites during hot deformation in addition to deformation conditions.

(2) During hot deformation of the composites containing Sc and Zr, Sc and Zr were in the supersaturated solid solution at low deformation temperature, while dynamic precipitation occurred at high deformation temperature.

(3) The activation energy map of the composites containing Sc and Zr can be divided in two regions. The activation energy decreases with increasing deformation temperature to the minimum level in the region I where the composites were in the solid solution condition. It follows by an increase with increasing temperature in the region II where dynamic precipitation occurred.

(4) Due to higher values of the activation energy in the region I, the composites containing Sc and Zr in the solid solution condition are more difficult to deform than that in the dynamic precipitation condition.

(5) Based on the combination of the activation energy map with the flow instability zone, the optimum hot workability of a composite in term of excellent processability was proposed at the domain (350–385 ℃ and 0.1–1 s^{-1} for S40 and 400–470 ℃ and 0.3–1 s^{-1} for SZ40), where the less energy of deformation was required.

Acknowledgments

The authors acknowledge the financial support of the Natural Sciences and Engineering Research Council of Canada (NSERC) and Rio Tinto Aluminum through the NSERC Industry Research Chair in the Metallurgy of Aluminum Transformation at the University of Quebec at Chicoutimi.

Conflict of interest

The authors declare no conflict of interest.

References

1. Bonnet G, Rohr V, Chen XG, et al. (2009) Use of Alcan's Al–B_4C metal matrix composites as neutron absorber material in TN International's transportation and storage casks. *Packag Transp Storage Secur Radioact Mater* 20: 98–102.
2. Fuller CB, Seidman DN, Dunand DC (2003) Mechanical properties of Al(Sc,Zr) alloys at ambient and elevated temperatures. *Acta Mater* 51: 4803–4814.
3. Lai J, Zhang Z, Chen XG (2012) The thermal stability of mechanical properties of Al–B_4C composites alloyed with Sc and Zr at elevated temperatures. *Mat Sci Eng A-Struct* 532: 462–470.
4. Lai J, Zhang Z, Chen XG (2013) Precipitation strengthening of Al–B_4C metal matrix composites alloyed with Sc and Zr. *J Alloy Compd* 552: 227–235.
5. Qin J, Zhang Z, Chen XG (2014) Effect of hot deformation on microstructure and mechanical properties of Al–B_4C composite containing Sc. *Mater Sci Forum* 794–796: 821–826.
6. Qin J, Zhang Z, Chen XG (2016) Mechanical Properties and Strengthening Mechanisms of Al-15 Pct B_4C Composites with Sc and Zr at Elevated Temperatures. *Metall Mater Trans A* 47: 4694–4708.
7. Qin J, Zhang Z, Chen XG (2017) Hot Deformation and Processing Maps of Al–15%B_4C Composites Containing Sc and Zr. *J Mater Eng Perform* 26: 1673–1684.
8. Qin J, Zhang Z, Chen XG (2017) Mechanical properties and thermal stability of hot-rolled Al–15%B_4C composite sheets containing Sc and Zr at elevated temperature. *J Compos Mater* 51: 2643–2653.
9. Sellars C, Tegart WMG (1966) Relation between flow stress and structure in hot deformation. *Mem Etud Sci Rev Met* 67: 731–746.
10. Shi C, Chen XG (2014) Effect of Zr addition on hot deformation behavior and microstructural evolution of AA7150 aluminum alloy. *Mat Sci Eng A-Struct* 596: 183–193.
11. Jin N, Zhang H, Han Y, et al. (2009) Hot deformation behavior of 7150 aluminum alloy during compression at elevated temperature. *Mater Charact* 60: 530–536.
12. Li Y, Liu Z, Lin L, et al. (2011) Deformation behavior of an Al–Cu–Mg–Mn–Zr alloy during hot compression. *J Mater Sci* 46: 3708–3715.

13. McQueen HJ, Spigarelli S, Kassner ME, et al. (2011) *Hot deformation and processing of aluminum alloys*, Boca Raton: CRC Press.
14. Shi CJ, Mao WM, Chen XG (2013) Evolution of activation energy during hot deformation of AA7150 aluminum alloy. *Mat Sci Eng A-Struct* 571: 83–91.
15. Shi C, Chen XG (2016) Evolution of activation energies for hot deformation of 7150 aluminum alloys with various Zr and V additions. *Mat Sci Eng A-Struct* 650: 197–209.
16. Wang S, Hou LG, Luo JR, et al. (2015) Characterization of hot workability in AA 7050 aluminum alloy using activation energy and 3-D processing map. *J Mater Process Tech* 225: 110–121.
17. Peng X, Su W, Xiao D, et al. (2018) Investigation on Hot Workability of Homogenized Al-Zn-Mg-Cu Alloy Based on Activation Energy and Processing Map. *JOM* 70: 993–999.
18. Malas JC, Venugopal S, Seshacharyulu T (2004) Effect of microstructural complexity on the hot deformation behavior of aluminum alloy 2024. *Mat Sci Eng A-Struct* 368: 41–47.
19. El-Danaf EA, AlMajid AA, Soliman MS (2008) Hot deformation of AA6082-T4 aluminum alloy. *J Mater Sci* 43: 6324.
20. Huang X, Zhang H, Han Y, et al. (2010) Hot deformation behavior of 2026 aluminum alloy during compression at elevated temperature. *Mat Sci Eng A-Struct* 527: 485–490.
21. Zhang H, Li L, Yuan D, et al. (2007) Hot deformation behavior of the new Al–Mg–Si–Cu aluminum alloy during compression at elevated temperatures. *Mater Charact* 58: 168–173.
22. Cerri E, Evangelista E, Forcellese A, et al. (1995) Comparative hot workability of 7012 and 7075 alloys after different pretreatments. *Mat Sci Eng A-Struct* 197: 181–198.
23. Johnson GR, Cook WH (1985) Fracture characteristics of three metals subjected to various strains, strain rates, temperatures and pressures. *Eng Fract Mech* 21: 31–48.
24. Samantaray D, Mandal S, Bhaduri AK (2010) Constitutive analysis to predict high-temperature flow stress in modified 9Cr–1Mo (P91) steel. *Mater Design* 31: 981–984.
25. McQueen HJ, Blum W (2000) Dynamic recovery: sufficient mechanism in the hot deformation of Al (<99.99). *Mat Sci Eng A-Struct* 290: 95–107.
26. Wouters P, Verlinden B, McQueen HJ, et al. (1990) Effect of homogenization and precipitation treatments on the hot workability of an aluminium alloy AA2024. *Mat Sci Eng A-Struct* 123: 239–245.
27. Prasad Y, Sasidhara S (1997) *Hot working guide: a compendium of processing maps*, ASM international.
28. Prasad Y (2003) Processing maps: a status report. *J Mater Eng Perform* 12: 638–645.

© 2019 the Author(s), licensee AIMS Press. This is an open access article distributed under the terms of the Creative Commons Attribution License (http://creativecommons.org/licenses/by/4.0)